Master's Thesis of Taehyeon Choi

Click Chemistry-based Liposome Nanoplatform for Macrophage Targeting and Depletion

대식세포 표적 및 제거를 위한 클릭 화학 기반 리포좀 나노플랫폼

August 2023

Graduate School of Convergence
Science and Technology
Seoul National University
Molecular Medicine and Biopharmaceutical Sciences

Taehyeon Choi

대식세포 표적 및 제거를 위한 클릭 화학 기반 리포좀 나노플랫폼

지도교수 임 형 준

이 논문을 이학석사 학위논문으로 제출함

2023년 7월

서울대학교 대학원

분자의학 및 바이오제약학과

분자의학 및 바이오제약학전공

최 태 현

최태현의 이학석사 학위논문을 인준함

2023년 7월

위 원 장	천 기 정	(인)
부위원장	임 형 준	(인)
위 원	이 윤 상	(인)

Click Chemistry-based Liposome Nanoplatform for Macrophage Targeting and Depletion

Taehyeon Choi

Submitting a Master's Thesis of Medicine

July 2023

Graduate School of Convergence
Science and Technology
Seoul National University
Molecular Medicine and Biopharmaceutical Sciences

Taehyeon Choi

Confirming the master's thesis written by
Taehyeon Choi
July 2023

Chair Gi Jeong Chen (Seal)
Vice Chair Hyung-Jun Im (Seal)
Examiner Yun-Sang LEE (Seal)

Abstract

Introduction: Immune checkpoint therapy using immune checkpoint inhibitors (ICIs) is a therapeutic method that induces anti-cancer immunity by activating immune cells within the tumor microenvironment (TME), rather than directly killing cancer cells. However, the clinical success of ICIs is that only about one-third of patients have sustained responses, but eventually recur. Therefore, various combination therapies have been studied to increase the therapeutic effect of ICIs. One of the notable combination therapies is to treat ICIs after modulating tumor-associated macrophages (TAMs) in the TME. Among the TAMs in the TME, M2 macrophages promote tumor growth. Agents used commercially to deplete such TAMs are Clodrosome® and m-Clodrosome®. However, the non-uniformity of these liposomal formulation-based drugs limits their clinical use. Therefore, we tried to develop a liposomal macrophage depleting agent that could target and deplete TAMs which is M2 macrophage and could be used clinically as a combination therapy with ICIs. The objective of this study was to prove the superiority of our developed liposomal macrophage depleting agent compared to Clodrosome® and m-Clodrosome®.

Methods: Click chemistry-based liposome nanoplatform was synthesized in two steps. First, liposomes were synthesized by a thin film hydration and extrusion. Second, the desired modalities including azide-functionalized chelator, mannose, fluorescence dye were conjugated with DBCO of liposomes using click chemistry

reaction. The biodistribution and macrophage depletion ability of functionalized liposomes were demonstrated in mice.

Results: We developed four types of click chemistry-based liposome nanoplatform that has a constant size and encapsulated with a clodronate for effective macrophage depletion, followed by conjugating Man-N_3 and metallic isotope ^{64}Cu labeling. Functionalization with Man-N_3 improve targeting ability of M2 macrophage and ^{64}Cu labeling enables in vivo positron emission tomography (PET) imaging of liposomes. Functionalized liposome nanoplatform was stable in physiological conditions and confirmed the difference of the biodistribution by using PET. Furthermore, clodronate-encapsulated mannosylated liposome (CML) among liposome nanoplatform effectively depleted M2 macrophages in normal liver and tumor microenvironment (TME) ex vivo compared to Clodrosome® and m-Clodrosome®.

Conclusions: Based on these finely tuned size control, high in vivo stability and excellent ex vivo M2 macrophage targeting and depleting effect, our liposome nanoplatform could be a promising macrophage depleting agent.

Keyword : Liposome, Macrophage, Clodronate, Molecular imaging, Click chemistry

Student Number : 2021-24307

Table of Contents

Chapter 1. Introduction

Immune checkpoint inhibitors (ICIs) that contain antibodies against programmed cell death protein 1 (PD1) or programmed death-ligand 1 (PD-L1) exert their anti-tumor effects by recovering T cells in the tumor microenvironment (TME) [1]. However, it has been reported that ICIs show response rates of 15-30% in the case of solid tumors, so they do not provide effective treatment to a large percentage of patients [2]. It is known to the limitations of these ICI therapeutic effects are closely related to Tumor-associated macrophages (TAM) in the TME. Therefore, as a proposal for improving the therapeutic effect of ICIs, a combination therapy of TAM modulation by TAM targeting and ICI agents is clinically evaluated [3, 4].

TAMs are the most abundant immune cells that promote tumor progression and angiogenesis in the TME [4]. Clodrosome® and m-Clodrosome® have been used to deplete TAMs [5, 6]. Clodrosome® and m-Clodrosome® are representative liposomal formulation-based drugs for macrophage depletion currently on the market. However, the measured hydrodynamic diameter of Clodrosome® and m-Clodrosome® is relatively non-uniform at 512.5±390.7 nm and 904.4±216.5 nm, respectively. Also, Each PDI was measured as 0.543 and 0.461. It is widely known that the particle size of liposomes affects hepatic uptake, pharmacokinetics, biodistribution, tissue diffusion and so on [7, 8]. Controlling and validating

parameters such as mean diameter, polydispersity index (PDI) is important for clinical applications of liposomal formulation-based drugs, so Clodrosome® and m-Clodrosome® are considered to be of limited clinical use [9].

Diverse nanoparticles such as liposomes [10, 11], albumins [12], antibodies [13], exosomes [14], iron oxide nanoparticles [15] have been investigated by many investigators. Particularly, liposomes have the advantage of being biocompatible, non-toxic, non-immunogenic, and biodegradable. Moreover, because phospholipid bilayer of liposomes is similar to a mammalian cell membrane, liposomes can be effectively cellular uptake due to the facilitation of cell-to-liposome interactions. Also, the ability of liposomes to encapsulate hydrophilic and hydrophobic active pharmaceutical ingredient (API)s can reduce the toxic effect of APIs and improve the circulation half-life of APIs by preventing drug degradation [7, 8, 16, 17]. Thus, liposomes were used as a drug delivery system (DDS) nanoplatform to effectively deliver clodronate that has an ability of macrophage depletion in this study [18-20].

Among TAMs in the TME, M2 macrophage promotes tumor angiogenesis and growth [21]. Therefore, we used mannose ligands to selectively target mannose receptors on the surface of M2 macrophages to enhance the effectiveness of macrophage depletion [22-24]. Accordingly, we would develop a macrophage depleting agent that can control TME by specifically targeting M2

macrophages, which are TAMs, and effectively reducing their numbers through this study.

Herein, we developed a click chemistry-based liposome nanoplatform that is uniformly sized and encapsulated with clodronate for effective macrophage depletion. The reason for using click chemistry as a surface modification tool is that liposomes can maintain their intrinsic properties during functionalization through site-specific conjugation. In particular, we used a SPAAC reaction which is not only copper-free and has a fast reaction rate, but also compatibility and bio-orthogonality in vivo [25-29]. To further explore efficacy of liposomes, we synthesized four different types of liposomes and confirmed the superiority of our liposomes through histological evaluation and efficacy evaluation (Scheme). Altogether, we believe that our liposome nanoplatform is superior in macrophage depletion effect compared to the already commercialized Clodrosome® and m-Clodrosome®.

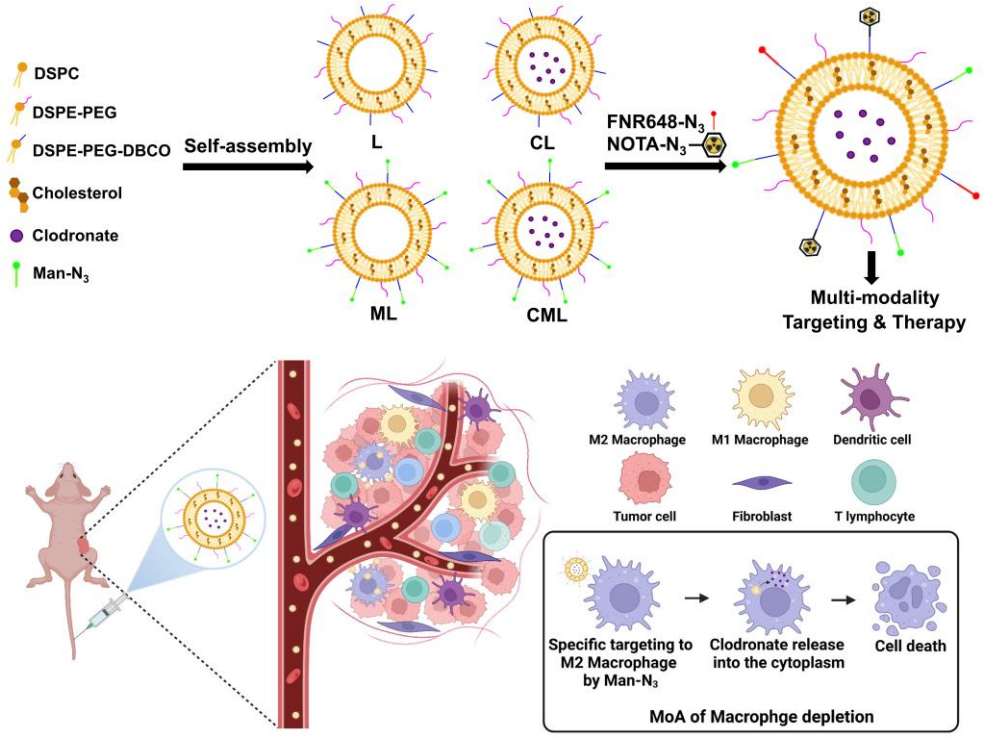

Scheme | Schematic illustration of multifunctional liposome nanoplatform synthesis and experimental design.

L: Liposome, ML: Mannosylated Liposome, CL: Clodronate encapsulated Liposome, CML: Clodronate encapsulated Mannosylated Liposome.

Chapter 2. Materials and Methods

2.1. Materials

Distearoyl phosphatidylcholine (DSPC), Cholesterol, 1,2-Distearoyl-sn-glycero-3-phosphoethanolamine(methoxy(polyethylene glycol)-2000) (DSPE-PEG(2k)), and 1,2-Distearoyl-sn-glycero-3-phosphoethanolamine-N-[dibenzocyclooctyl(polyethylene glycol)-2000] (DSPE-PEG(2k)-DBCO) were purchased from Avanti Polar Lipids Inc. (Alabama, USA). Disodium Clodronate Tetrahydrate was purchased from Tokyo Chemical Industry Co., LTD. (Tokyo, Japan). Clodrosome® and m-Clodrosome® were purchased from Encapsula Nano Sciences (Nashville, TN, USA). 2,2',2″-(2-(4-(3-(3-azidopropyl)thioureido)benzyl)-1,4,7-triazonane-1,4,7-triyl)triacetic acid (NOTA-N3) and azido-Flamma 648 (FNR648-N3) were purchased from FutureChem (Seoul, Korea). 1,1′-Dioctadecyl-3,3,3′,3′-tetramethylindocarbocyanine perchlorate (DiI) were purchased from Invitrogen (Carlsbad, USA). 1-O-(2-(2-(2-azidoethoxy)ethoxy)ethoxy)-alpha-D-mannopyranoside (Man-N3) was purchased from Iris Biotech GmbH (Marktredwitz, Germany). All other reagents and chemicals were purchased from Sigma-Aldrich (St. Louis, MO, USA). Size exclusion PD-10 column was purchased from GE Healthcare Life Science (Buckinghamshire, UK). Instant thin-layer chromatography-silica gel (ITLC-SG)

plates were purchased from Agilent Technologies, Inc. (Santa Clara, CA, USA).

2.2. Liposome preparation

A standard thin film hydration method was employed for liposome synthesis. DSPC, Cholesterol, DSPE-PEG(2k) and DSPE-PEG(2k)-DBCO (10.6:7.2:1:1 in a molar ratio) were dissolved in the mixture of chloroform and methanol. The mixture was evaporated using N_2 gas until a thin lipid film was formed. Following evaporation, the lipid film was vacuumed for 4 h to remove the remaining residual organic solvents inside lipid layer. The lipid film was hydrated with D.W (1 mL) contained of clodronate (20 mg, 55.4 umol) and dispersed by vortexing and sonication. The liposomal solution was extruded using polycarbonate track etch (PCTE) membrane filter to obtain the desired size. The liposome was ultrafiltrated with Amicon Ultra 100 kDa filter centrifuge tubes for 5 min at 10000 rpm. To obtain fluorescence conjugated liposomes, FNR648-N3 (7.67 ug, 10 nmol) or DiI (9.3 ug, 10 nmol) was added and incubated at 4℃. This conjugate was further purified using a PD-10 column to purify it from free FI. For liposome conjugates with targeting moiety, targeting compound of Man-N_3 was added by half the amount of PEG. This conjugate was also purified using a PD-10 column.

2.3. Characterization of liposomes

The hydrodynamic diameter and size distribution of the liposomes diluted 50-fold using D.W was measured using dynamic light scattering and nanoparticle tracking analysis (DLS and NTA, Malvern Instruments Ltd., Worcestershire, UK). The morphologies of liposomes were observed using a transmission electron microscope (TEM, JEM-1400, JEOL, USA). To prove the stabilities in physiological conditions, stability tests of liposomes were conducted in phosphate buffered saline (PBS), human serum, and cell media (DMEM) at the different time points (0, 1, 7, and 14 d). The absorbance at 309 nm was measured by NanoDrop® ND-1000 (NanoDrop Technologies, Wilmington, DE, USA) to confirm absorbance peak of DBCO.

2.4. Radiolabeling of liposomes and the stability test

The vial containing ^{64}Cu was dried by N_2 gas in fume hood for 30 min. After that, 200 uL of 1 M sodium acetate buffer (pH 5) was added to the vial to adjust pH 5. NOTA-N_3 (10 ug, 18 nmol) dissolved in D.W (10 uL) was added and heated at 70℃ for 5 min. Finally, 10 uL of [^{64}Cu]Cu-NOTA-N_3 was added to liposomes in PBS and incubated overnight at 4℃. To remove unchelated free ^{64}Cu ion, ^{64}Cu-labeled liposomes through click chemistry were purified using the PD-10 column eluted with PBS. Thin-layer

chromatography (TLC) was conducted with ITLC-SG paper using citric acid (0.1 M) as the mobile phase to determine the radiolabeling efficiency. The R_f values of the free ^{64}Cu, [^{64}Cu]Cu-NOTA-N_3, and ^{64}Cu-labeled liposomes were 0.9~1.0, 0.7~0.8, and 0.0~0.1, respectively (**Fig. 1**).

To demonstrate radiostability, ^{64}Cu-labeled liposomes were diluted 10-fold using human serum. Radiolabeling efficiency of ^{64}Cu-labeled liposomes dissolved in PBS and human serum was measured at each time point (0, 12, and 24 h), respectively to confirm the stable conjugation of the radiolabeled agent during the imaging procedure.

2.5. Determination of the clodronate encapsulation efficiency

In the process of ultrafiltration of liposomes using an Amicon Ultra 100 kDa filter centrifuge tubes, the solution that came down the filter was taken [30]. The absorbance at 205 nm was measured to determine the concentration of clodronate in the solution. Finally, EE% was calculated from the equations below:

$$EE\% = \frac{\text{Total amount of drug} - \text{unencapsulated drug}}{\text{Total amount of drug}} \times 100$$

2.6. Cell viability test

RAW264.7 cells (2×10^4 per well) in 200 uL of DMEM containing 10% FBS and 1% penicillin/streptomycin (PS) were seeded onto 96-well plates and incubated at 37℃ for 24 h. After removal of media, liposomes were added to each well with different concentration of clodronate (100, 200, and 400 ug/mL) and incubated at 37℃ for 24 h. The control group was cells without any treatment of liposomes. After 24 h, media was removed and CCK-8 reagent (Dojindo, Japan) was added to wells. Afterwards, it was incubated at 37℃ for 2 h. The absorbance signals of each well were measured with a GLOMAX Multi Detection System (Promega BioSystems Sunnyvale, California, USA) at 450 nm. The viability was calculated as a percentage to absorbance of control cells.

2.7. Cellular uptake study

RAW264.7 cells were cultured at 10^5 cells in 12-well dishes and incubated at 37℃ for 24 h. The DMEM medium containing 10% FBS and 1% PS was used for the experiment. After removal of media, liposomes were added to each well with 200 ug/mL of clodronate and incubated at 37℃ for 4 h. After the incubation, cells were washed with DPBS three times. Then, 4% PFA was added to fix cells and incubated at 37℃ for 10 min. Cells were washed with DPBS three times. Finally, cells were stained using mounting medium with DAPI and fixed on a slide glass through a cover glass. All observations were performed using a laser scanning confocal

microscope (LSM800, Carl Zeiss, Oberkochen, Germany).

2.8. In vivo PET imaging

Six-week-old male mice (C57BL/6) were purchased from Koatech (Pyeongtaek, Korea). Approximately 1.85 MBq of ^{64}Cu-labeled liposomes with clodronate (500 ug, 1.39 umol) was injected intravenously into seven-week-old normal mice (C57BL/6) anesthetized with 2% isoflurane. Clodronate-free liposomes (L and ML) were injected by matching the number of liposome particles to that of clodronate encapsulated liposomes (CL and CML). The PET scan images were acquired at the different time points (0, 2, 8, and 24 h) after injection using a preclinical PET/X-ray scanner (GENISYS4, Sofie Bioscience, California, USA). PET imaging processing was conducted by InVivoScope software (version 2.0). The region of interest (ROI) was calculated using AMIDE software when calculating the quantitative evaluation in the uptake of blood pool and liver. The time activity curve was fitted based on %ID/g at each time point.

2.9. Biodistribution analysis

The biodistribution of ^{64}Cu-labeled liposomes was evaluated in normal mice (C57BL/6). Approximately 0.2 MBq of ^{64}Cu-labeled liposomes with clodronate (500 ug, 1.39 umol) was injected through

the tail vein of seven-week-old normal mice. Clodronate-free liposomes (L and ML) were injected the same way as the PET imaging process. The animals were sacrificed and dissected for various organs (blood, intestine, spleen, stomach, liver, kidney, heart, and lung) at the different time points (0, 2, 8, and 24 h) after tail vein injection. Radioactivity was measured using an automatic gamma counter (Wizard, PerkinElmer, USA). Counts per minute were decay-corrected, and the results were expressed as %ID/g.

2.10. Ex vivo tissue fluorescence imaging

5 mg/mL DiI-labeled Clodrosome® and m-Clodrosome® (0.1 mL), DiI-labeled CL and CML with clodronate (500 ug, 1.39 umol, 0.1 mL) were injected to normal mice (C57BL/6) through tail vain. Also, DiI-labeled L and ML were injected with the same number of particles as DiI-labeled CL and CML. The animals were sacrificed and dissected for liver at 24 h after injection. The liver was molded using OCT compound at -20 ℃. Molded liver was cut with a Leica CM1860 cryostat (Leica Biosystems, Wetzlar, Germany) and obtained liver tissue slice was placed on a slide glass. After staining the liver tissue slice using mounting medium with DAPI, it was covered with a cover glass. Fluorescence images were acquired using a LSM800 laser scanning confocal microscope.

2.11. Tumor modeling

4T1 breast cancer bearing mice were used for efficacy evaluation. 4T1 cell line (5×10^5 cells 100 uL^{-1} of normal saline) was injected into the right flank. Efficacy evaluation with 4T1-bearing mice was conducted when the implanted 4T1 tumor reached approximately 200 mm^3.

2.12. Immunohistochemistry

Normal mice (C57BL/6) were intravenously injected with 0.1 mL of 5 mg/mL Clodrosome® and m-Clodrosome®, 0.1 mL of CL and CML with clodronate (500 ug, 1.39 umol), respectively. The number of injected liposomal particles for clodronate-free liposomes (L and ML) was the same as for clodronate encapsulated liposomes (CL and CML). The animals were sacrificed and dissected for liver at 24 h after injection. 4T1-bearing mice were intravenously injected as single dose with the same amount of normal saline, CL, CML, Clodrosome®, m-Clodrosome® that injected into normal mice. The animals were sacrificed after 2 weeks of follow-up and dissected for tumor. Formalin-fixed and paraffin-embedded liver and tumor tissues were cut into 4 um thick sections and automatically stained with rabbit anti-CD206 antibody (1:1000, Abcam) using standard protocols on the Ventana Discovery XT automated immunohistochemistry system (Roche,

Switzerland). Stained slides were imaged using a Leica SCN400F slide scanner (Leica Microsystems, Germany) at 400× magnification. After immunohistochemistry, H&E staining was also conducted to observe histological abnormalities.

2.13. Statistical Analysis

All statistical analyses were conducted by the GraphPad Prism software (version 5.0) and displayed as the mean ± standard deviation (SD). The means were compared using the one-way ANOVA followed by Tukey post hoc test. P-values < 0.05 were considered statistically significant and were represented by *, $P < 0.05$; *, $P < 0.01$; **, $P < 0.001$; ***.

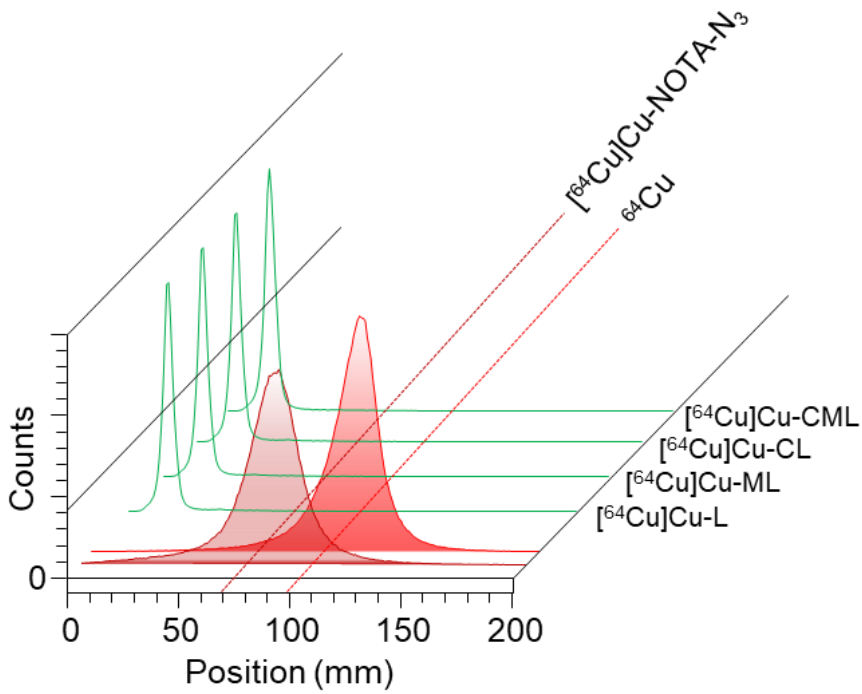

Fig. 1 | Labeling efficiency of all the liposomes.

Labeling efficiency of all the liposomes used in experiments was assessed after click chemistry with [^{64}Cu]Cu−NOTA−N_3. The radiochemical purity of all the liposomes was determined using radio TLC chromatogram and percentage of value at R_f = 0.0~0.1.

Chapter 3. Results and Discussions

3.1. Liposome nanoplatform characterization

Conventionally, Doxil®, the first FDA-approved liposomal drug, as well as FDA-approved or currently being investigated liposomal drugs are typically designed at 100 nm diameters [8, 31]. The reason is that most therapeutic liposomes usually aim to avoid mononuclear phagocytic system (MPS) uptake and increase blood circulation time [7]. Also, previous papers argue that nanoparticles bigger than 100 nm cannot pass through hepatocytes, because the hepatic fenestration of endothelium is approximately 100 nm [32, 33]. For these reasons, we decided to synthesis 100 nm liposome nanoplatform. The hydrodynamic diameters of liposomes (L, ML, CL, and CML) were 90.85±15.69, 93.44±32.18, 99.79±17.96, and 101.8±24.4 nm, respectively (**Fig. 2a**). All liposomes had a PDI value of around 0.2, suggesting that the liposomes have a homogenous population [9]. The zeta potential tended to be slightly higher with Man-N_3 binding through click chemistry; however, the results were within the margin of error. On the contrary, Clodrosome® and m-Clodrosome® had a large standard deviation in size, and PDI was 0.543 and 0.461, respectively. This result suggests that they are relatively heterogenous population (**Table 1**). These tendencies were also confirmed by the results that all

liposomes formed a single peak, whereas Clodrosome® and m-Clodrosome® formed multiple peaks in NTA analysis (**Fig. 3**). The liposome nanoplatform was revealed that it has a spherical shape and uniform size distribution by TEM (**Fig. 2b**). The stabilities of the liposomes were assessed in various physiological solutions (PBS, human serum, and cell media) to determine the feasibility of in vivo utilization of them. The hydrodynamic diameters of the liposomes were maintained within 20% error margin for 14 d (**Fig. 2c**). Additionally, it was confirmed that they showed no visible aggregates or precipitates for 14 d (**Fig. 4**). The UV-visible spectrum showed peak intensities at specific wavelengths for DBCO (peak intensity at 309 nm, yellow square box) (**Fig. 2d**). This result proves that DBCO as a click chemistry derivative appears on the surface of the liposome. The radiochemical stabilities were over 95% for up to 24 h in PBS and human serum, implicating that in vivo utilization of the liposome nanoplatform would be effective (**Fig. 1e**). Clodronate encapsulation efficiency was no difference between CL and CML (**Fig. 1f**). In further experiments, the results that the clodronate encapsulation efficiency did not significantly decrease even after 30 days from the synthesis of the liposomes (CL and CML) indicated that clodronate was released from the liposomes in a sustained release form (**Fig. 5**).

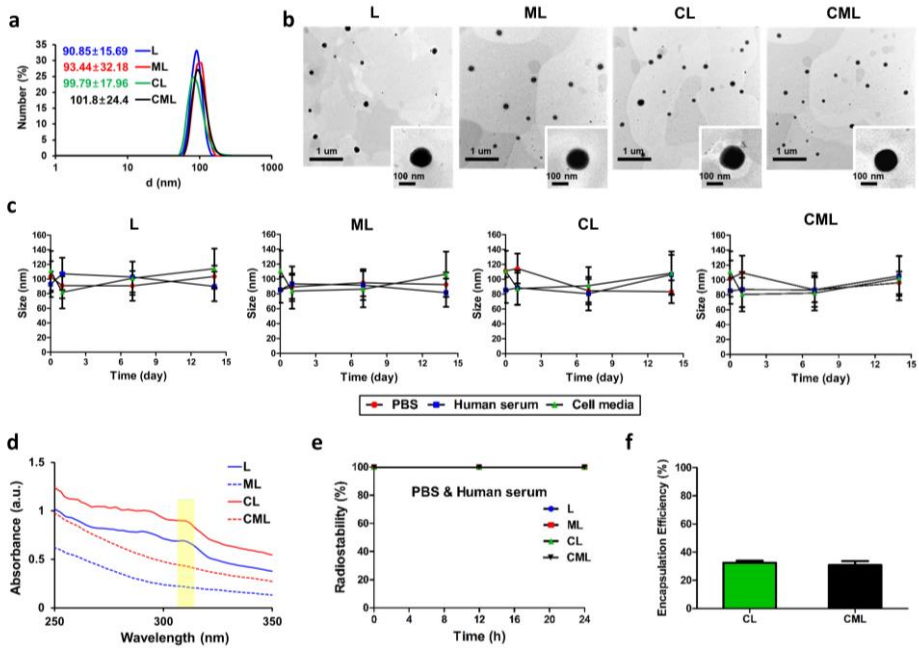

Fig. 2 | Characterization of Liposome nanoplatform for Macrophage depletion.

a, Hydrodynamic diameter of liposomes. All data were averaged by five measurements using the DLS system.

b, TEM images of liposome nanoplatform with low and high magnifications (down) respectively.

c, Stability test of liposome nanoplatform in physiological solutions (PBS, human serum, and cell media) for 14 d.

d, UV spectrum of peak change according to binding of Man−N_3 to liposomes.

e, Radiostability test in PBS and human serum at each time point (0, 12 and 24 h) after radiolabeling through click chemistry.

f, Clodronate encapsulation efficiency of CL and CML (n = 3, mean ± SD). * : $P < 0.05$, **: $P < 0.01$.

Sample	Size (nm)	Poly dispersity index (PDI)	Zeta-potential (mV)
L	90.85±15.69	0.114	-23.6±8.06
ML	93.44±32.18	0.221	-21±7.43
CL	99.79±17.96	0.196	-21.3±4.72
CML	101.8±24.4	0.239	-21±5.04
Clodrosome	512.5±390.7	0.543	-5.86±5.13
m-Clodrosome	904.4±216.5	0.461	-3.12±3.86

Table 1. | Size and zeta potential of samples

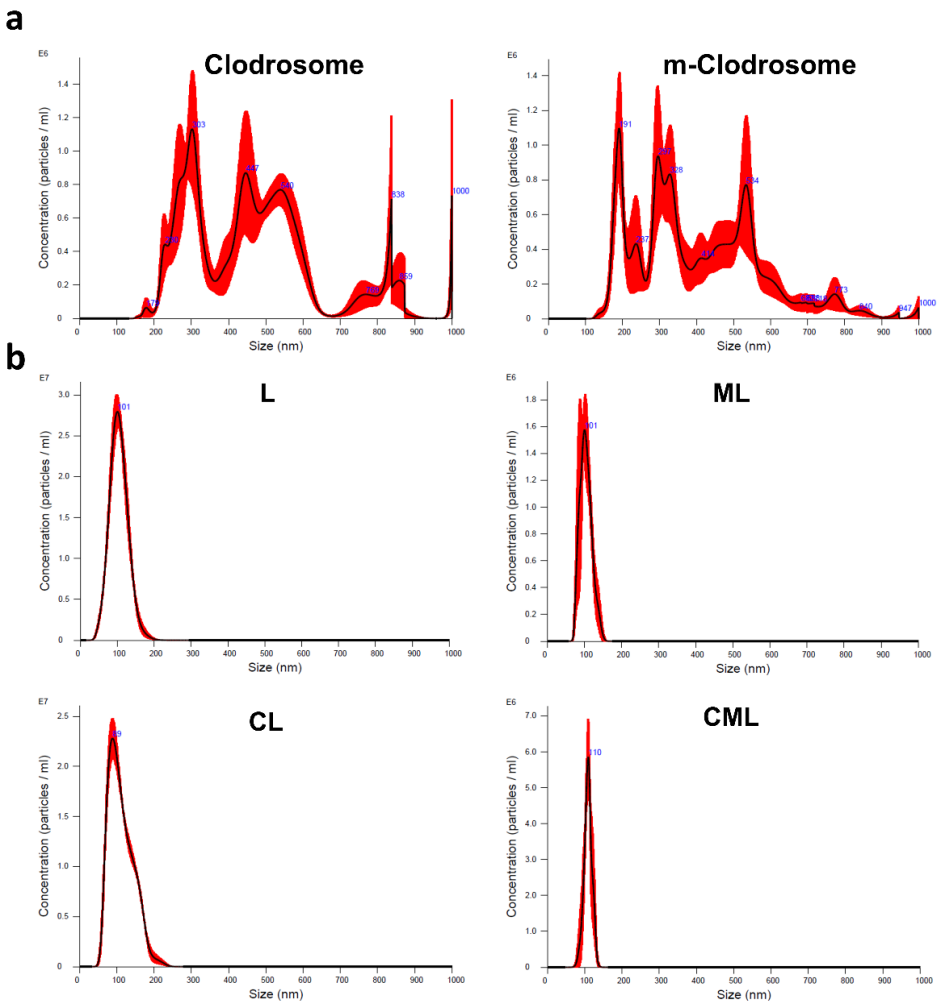

Fig. 3 | NTA analysis of Liposomes.

a, The size distribution of Clodrosome and m-Clodrosome.

b, The size distribution of liposome nanoplatforms in PBS was measured using the NTA system.

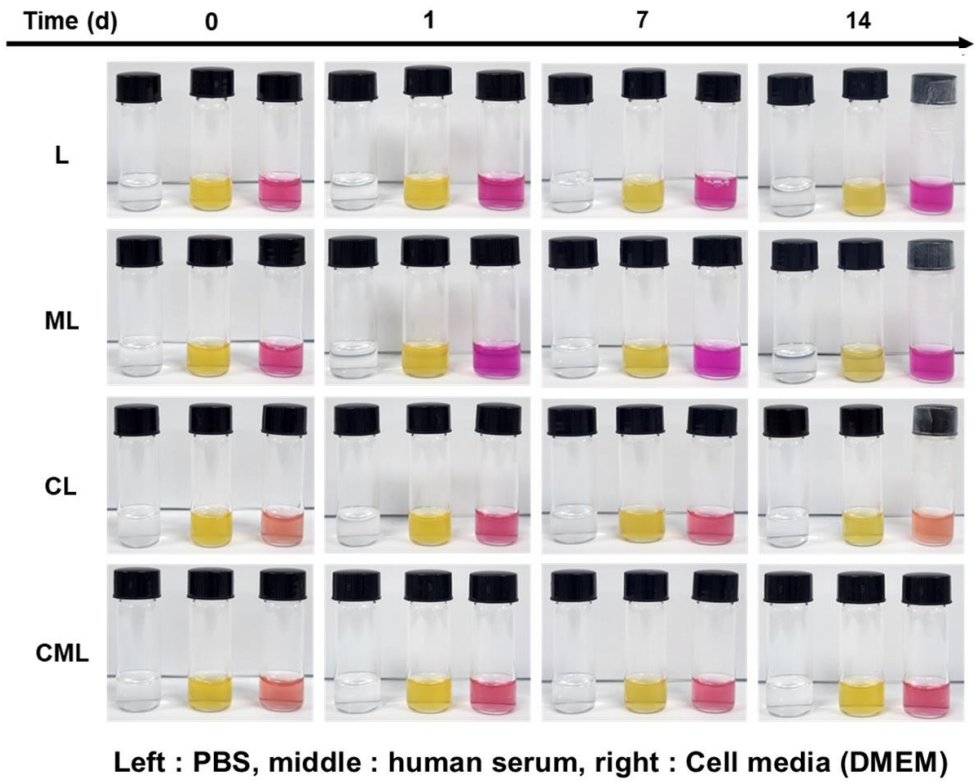

Fig. 4 | Stability test of Liposomes in the different physiological conditions (PBS, human serum, and Cell media (DMEM).

No visible aggregates and precipitates of the liposomes were observed in all liposome experimental groups for 14 d.

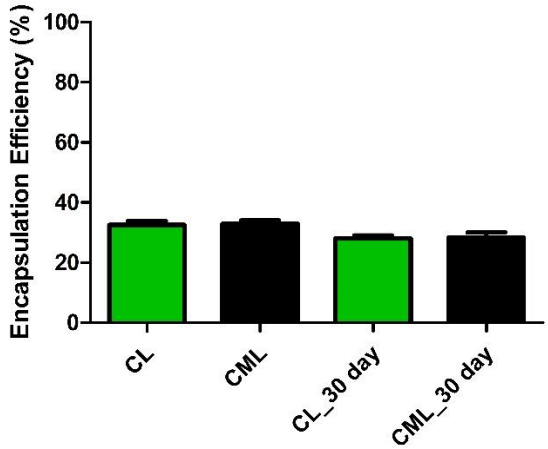

Fig. 5 | Clodronate releasing test.

Clodronate encapsulation efficiency of liposomes was measured by Nanodrop. All groups were not significant. Statistical analysis was conducted by one-was ANOVA test.

3.2. In vitro cell viability test of Liposome nanoplatform for Macrophage depletion

The cell viability test of liposome nanoplatform were assessed to determine the toxicity on a cellular level (**Fig. 6a**). All experiments were performed with RAW264.7 cell. Clodronate-free liposomes (L and ML) did not affect cell viability to the control group, RAW264.7 cell. This suggests that the liposomes we synthesized are reasonably biocompatible. On the other hand, clodronate encapsulated liposomes (CL and CML) decreased cell viability by clodronate in a dose dependent manner. Particularly, this tendency was shown to be significantly higher in CML than CL at clodronate concentration of 100, 200, and 400 ug/mL ($P < 0.05$, $P < 0.01$, and $P < 0.001$, respectively). Meanwhile, it was confirmed that our liposomes do not show significant differences when compared to Clodrosome® and m-Clodrosome® in terms of cytotoxicity (**Fig. 7**).

3.3. In vitro cellular uptake test of Liposome nanoplatform for Macrophage depletion

The cellular uptake liposome nanoplatform was observed in the red fluorescence images to assess the degree of specific binding to RAW264.7 cell (**Fig. 6b**). First, when we investigated at the tendency of liposomes to cell uptake through several time points (0.5, 1, 2, 4, and 24 h), cell uptake was well achieved at 4 h (**Fig. 8**).

Fluorescence signal of the mannosylated liposomes (ML and CML) was significantly higher than that of mannose-free liposomes (L and CL). This result implies that the mannosylated liposomes were specifically bound to the cells by the targeting ligand, the mannose ligand. In addition, it was demonstrated that RAW264.7 cells do not cause autofluorescence in the FNR648-N_3 wavelength band (Ex/Em: 648/663 nm) through the absence of red fluorescence from cells not treated with liposomes.

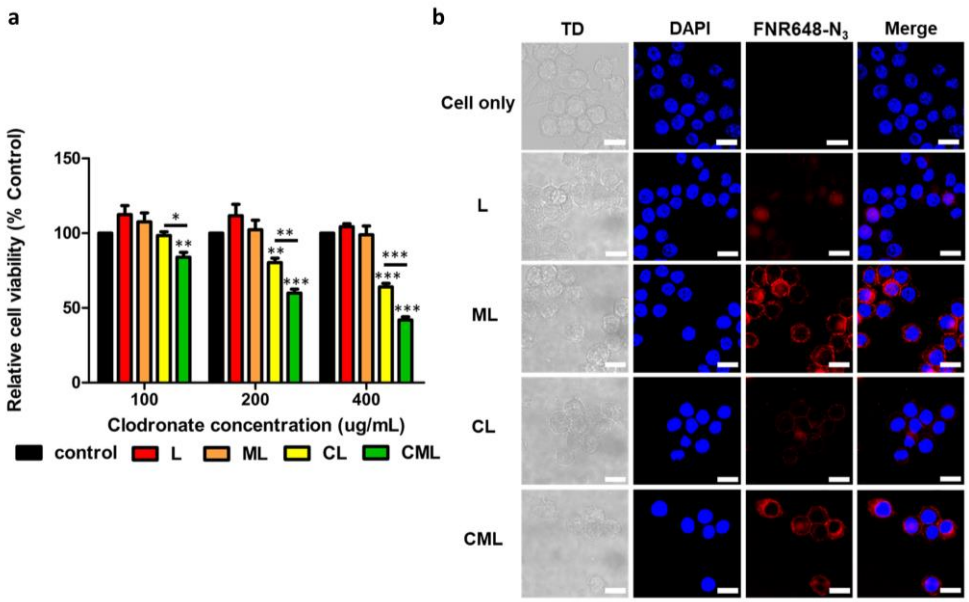

Fig. 6 | Cell viability and Cellular uptake of Liposome nanoplatform for Macrophage depletion.

a, Cell viability test was performed using a CCK assay with RAW264.7 cells at different concentration of clodronate. (n = 3, mean ± SD). * : P <0.05, ** : P <0.01, *** : P < 0.001.

b, In confocal microscopy, mannosylated liposomes (ML and CML) internalized in RAW264.7 cells while L and CL showed minimal internalization. All scale bars in the images are 75 um. TD: transmitted light channel, blue: nuclei (DAPI), red: fluorescence conjugated liposomes (FNR648-N_3).

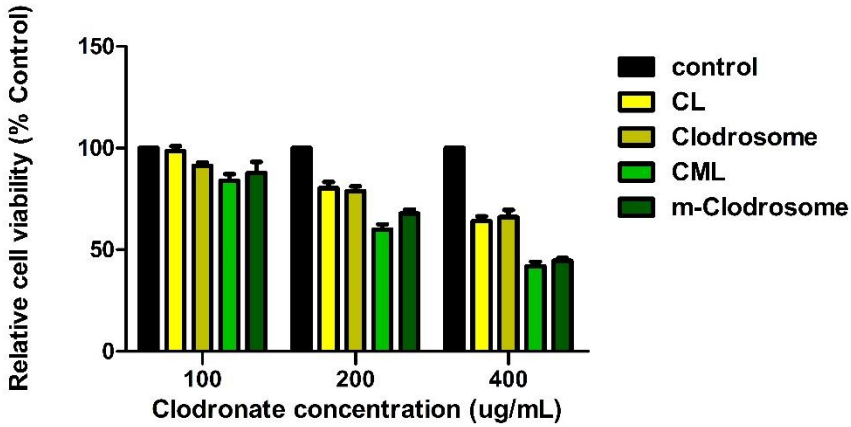

Fig. 7 | Cell viability test of RAW264.7 treated liposomes.

Comparison of liposomes with Clodrosome and m-Clodrosome. All groups were not significant. Statistical analysis was conducted by one-was ANOVA test.

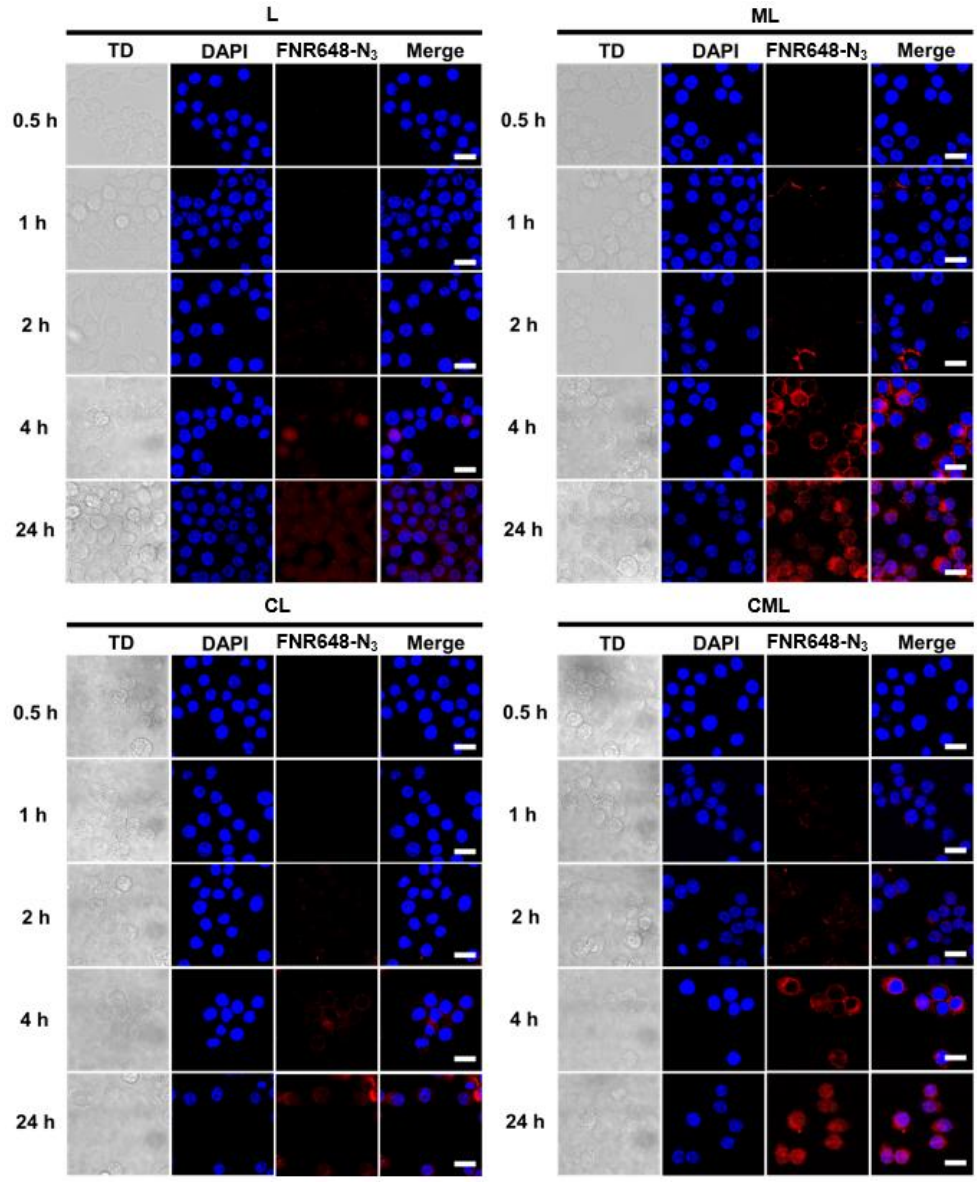

Fig. 8 | Cell uptake test of liposomes in RAW264.7.

Comparison of cellular uptake of liposomes at several time points (0.5, 1, 2, 4, and 24 h). All scale bars in the images are 75 um.

3.4. Pharmacokinetics and ex vivo biodistribution of Liposome nanoplatform

We performed biodistribution studies of liposome nanoplatform by using PET imaging analysis to determine the changes of distribution in the body over time. The biodistribution of liposomes was significantly different by clodronate (**Fig. 9a**). Clodronate-encapsulated liposomes (CL and CML) had a shorter blood circulation time than clodronate-free liposomes (L and ML) at all time points, but the liver uptake was higher and longer. In addition, mannosylated liposomes (ML and CML) were higher and longer liver uptake at all time points compared to mannose-free liposomes (L and CL). Furthermore, the signals observed in the liver are speculated to be solely due to liposomes. Since the liposomes were labeled with ^{64}Cu and injected after purification through a PD-10 column, it is estimated that there is no free ^{64}Cu. Additionally, according to S Ait-Mohand, ^{64}Cu-NOTA-N_3 is highly stable in vivo by 1200 min, and there have been reports stating that ^{64}Cu chelated to NOTA does not undergo demetallation and does not come out of the NOTA cavity [34]. Meanwhile, all experimental groups exhibited a weak signal in the gallbladder, estimating the uptake of liposomes by kupffer cells. First, if the liposomes were taken up by hepatocytes, it is expected that they would be excreted through the hepatobiliary tract via the gallbladder and intestine. However, in this study, no uptake of liposomes was observed in the gallbladder or

intestine [35]. Second, kupffer cells are a type of liver-resident macrophages that play an important role in innate immune responses and are located in the lumen of the liver sinusoid. Furthermore, since kupffer cells constitute MPS, they participate in liver metabolic function by efficiently phagocytizing liposomes that enter via the sinusoidal blood [36-38]. Third, nanoparticles smaller than 100 nm can pass through hepatocytes due to the size of the endothelium of hepatic fenestrations as mentioned above [32, 33]. Therefore, our liposomes may have been internalized into Kupffer cells rather than hepatocytes, according to several arguments. Moreover, these biodistribution tendencies were appeared in the time activity curve quantitatively analyzed on a PET image basis (**Fig. 9b and Table 2**). At 0 h and 8 h in the blood pool, L was the highest at 43.23±4.84% ID/g and 21.67±4.57% ID/g, respectively, which was two to four times higher than the values of CL and CML at the same time points. CML was the highest liver uptake among liposomes. It was 61.78±4.06% ID/g at 8 h, which was 2.7, 2.0, and 1.2 times higher than L, ML, and CL in the same time point, respectively. This result will later serve as the basis for functional evaluation experiments as an immunosuppressive drugs through the changes in the number of kupffer cells, which are macrophages in the liver. Furthermore, the biodistribution tendency of liposome nanoplatform was also confirmed through ex vivo biodistribution analysis. Clodronate encapsulated liposomes (CL and CML) were highly accumulated at liver and spleen. they showed similar increases in spleen uptake over time, with the highest tendency at 8

h. This tendency appeared to be same for liver uptake (**Fig. 10a**). One of the reasons for these results is that liver and spleen present sensitive blood irroration and have various type of tissue-resident macrophages [31, 39]. Especially, because CL and CML were irreversibly sequestered by MPS due to the clodronate which is API, they seem to be highly accumulated by MPS (i.e., liver and spleen) [40]. It was confirmed that the tendency for liver and spleen to uptake more CL and CML was the same when comparing % ID/g of L and the rest of the experimental groups (**Fig. 10b**). Thus, we decided to prove how effectively liposome nanoplatform deplete macrophages in vivo.

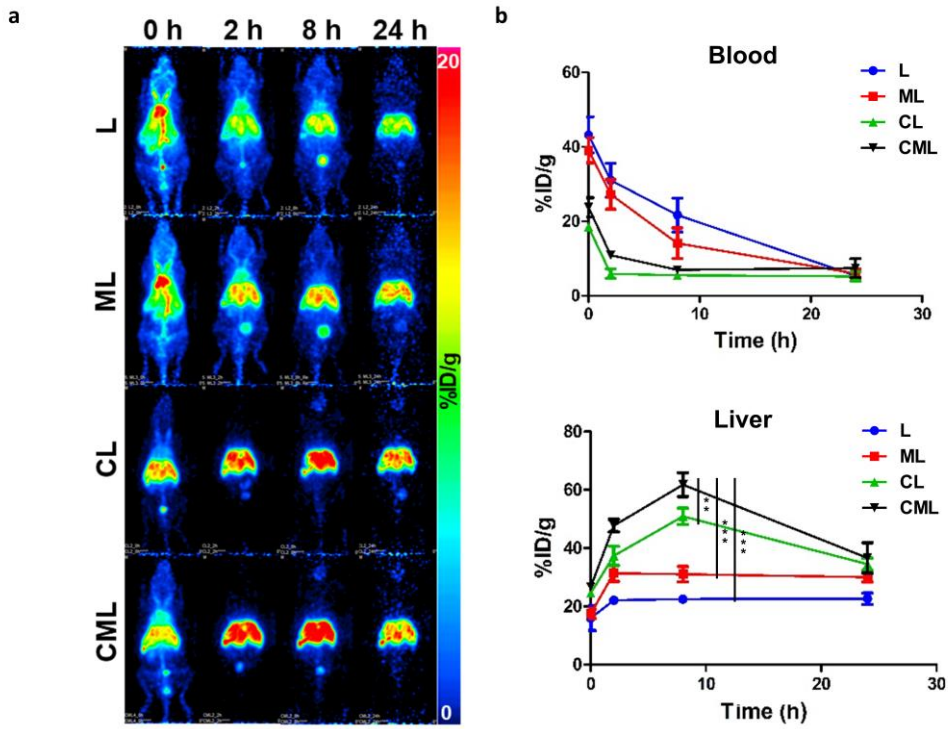

Fig. 9 | in vivo PET imaging of Liposome nanoplatform for Macrophage depletion.

a, Representative PET images of normal mice (n = 3) at the different time points (0, 2, 8, and 24 h) after tail vein injection of ^{64}Cu-labeled liposomes (L, ML, CL, and CML).

b, Time activity curve of the blood pool and liver (n = 3, mean ± SD). **: P < 0.01, ***: P < 0.001.

		Blood pool (% ID/g)		Liver (% ID/g)	
		Average	SD	Average	SD
L	0 h	43.23	4.84	15.97	4.24
	2 h	31.01	4.57	22.09	1.55
	8 h	21.67	4.57	22.50	1.27
	24 h	5.37	0.97	22.61	1.96
ML	0 h	39.10	3.37	17.52	1.59
	2 h	27.21	3.97	31.38	2.75
	8 h	14.08	4.12	31.04	2.64
	24 h	5.96	1.26	30.02	1.64
CL	0 h	18.45	0.72	24.58	1.38
	2 h	5.88	1.27	37.35	3.28
	8 h	5.46	1.00	50.90	2.80
	24 h	5.18	1.26	34.50	2.10
CML	0 h	23.75	2.62	26.72	1.36
	2 h	10.89	0.95	47.73	2.17
	8 h	6.93	0.53	61.78	4.06
	24 h	7.43	2.50	36.63	5.19

Table 2. | Quantified organ uptakes of Liposomes measured using PET imaging (n = 3 for each group)

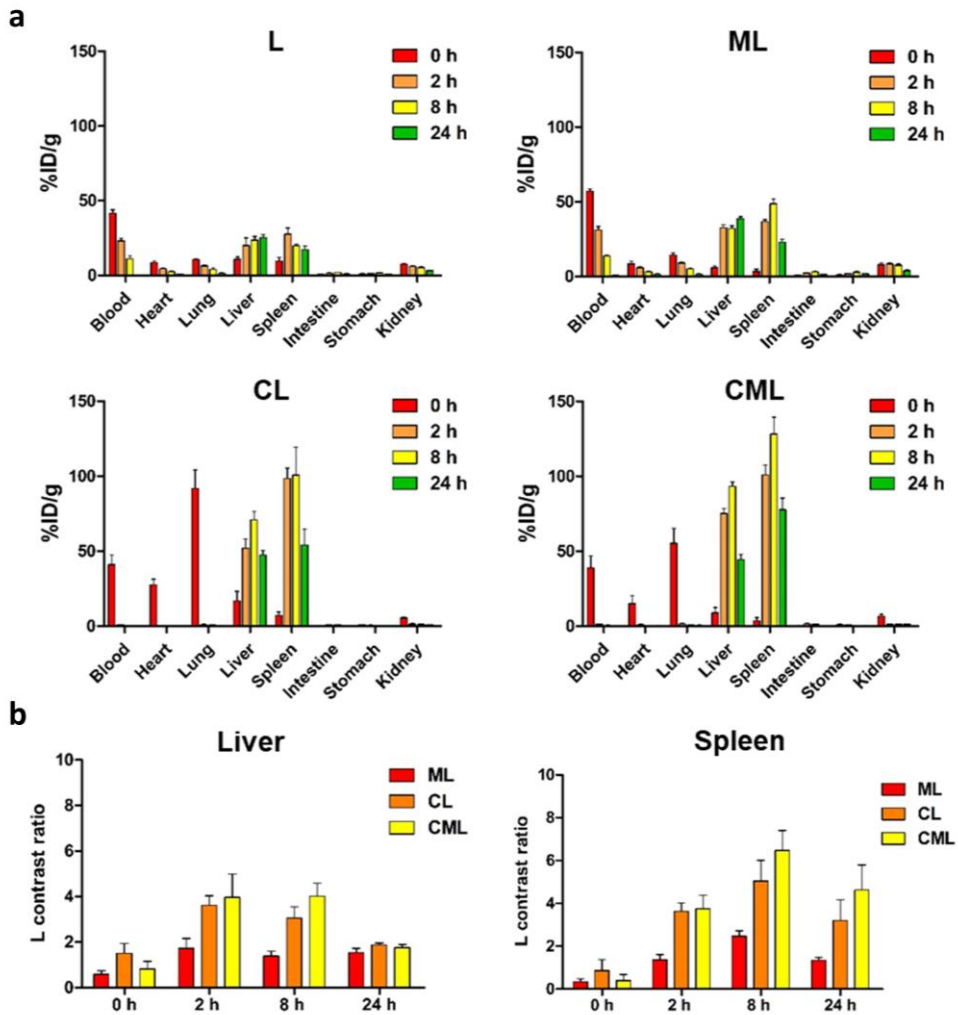

Fig. 10 | Quantitative analysis of Liposome nanoplatform for Macrophage depletion.

a, Quantitative analysis of liposomes in various organs of normal mice, expressed as % ID/g. (n = 4, mean ± SD).

b, Comparison of relative uptake of liposomes in liver and spleen (n = 4, mean ± SD).

3.5. Immunological function evaluation of liposome nanoplatform for macrophage depletion in liver tissue ex vivo

To determine in vivo injected liposomes effectively deplete macrophages in liver tissues compared to positive controls (i.e., Clodrosome® and m-Clodrosome®), we dissected liver tissues and performed histological evaluations. First, green fluorescence images from confocal microscopy were used to compare the ability of macrophage depletion (**Fig. 11**). It was showed that the green fluorescence signal of CML was the lowest among all experimental groups including the positive controls, speculating that the greatest number of macrophages in liver tissue decreased. Then, immunohistochemistry was conducted using anti-CD206 antibody as M2 macrophage marker to analyze more histologically [41]. The expression level of the M2 macrophage surface marker CD206 was the lowest in CML among all experimental groups (**Fig. 12**). Two reasons can be presented for this result. First, the expression of mannose receptor is increased in M2 macrophages [41]. The mannose receptor contains carbohydrate-recognition domain 4 (CRD_4), and the mannosylated nanoparticles can be specifically internalized to the M2 macrophages due to the high-affinity binding between CRD_4 and the mannosylated nanoparticles [24]. Thus, as mannose receptors increase, more mannosylated nanoparticles can be internalized to the M2 macrophages via increased CRD_4. Second,

CML is uniform at 100 nm, but the positive controls are more than 500 nm in particle size and are non-uniform. Kupffer cells phagocytize nanoparticles mainly using a clathrin-mediated endocytosis when internalizing nanoparticles through mannose receptors. Clathrin-mediated endocytosis is known to have the internalization of size range of about 100-350 nm. Meanwhile, kupffer cells also phagocytize nanoparticles through macropinocytosis which is responsible for 0.5-5 um internalization, but macropinocytosis rarely occurs [36, 42]. In other words, it can be inferred that CML might be efficiently internalized kupffer cells via clathrin-mediated endocytosis, unlike the positive controls. Therefore, our histological evaluation in liver tisssues can be explained that CML which has a constant size of 100 nm might be internalized by clathrin-mediated endocytosis to M2 macrophages with overexpressed mannose receptors on the surface compared to the positive controls, and induced apoptosis by clodronate for M2 macrophage depletion. Additionally, H&E staining was performed to confirm that the liposomes caused histological damages to the liver. (**Fig. 13**). There was no significant difference in the shape of the nucleus and cytoplasm of hepatocytes in all experimental groups in comparison with the control group. This result proved that liposomes had no hepatotoxicity.

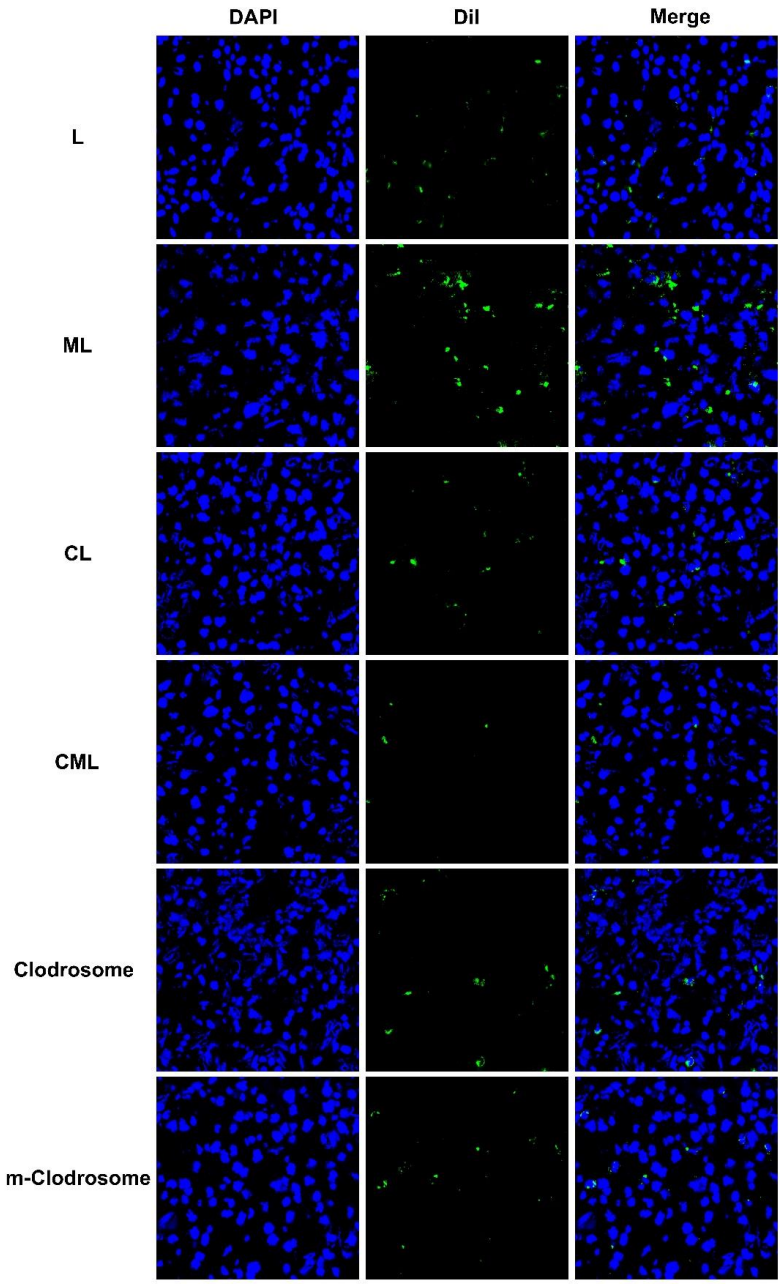

Fig. 11 | Confocal images of the liver tissue treated liposomes.

Ex vivo tissue fluorescence images acquired 24 h post-injection of liposomes with a normal mice. All scale bars in the images are 250 um.

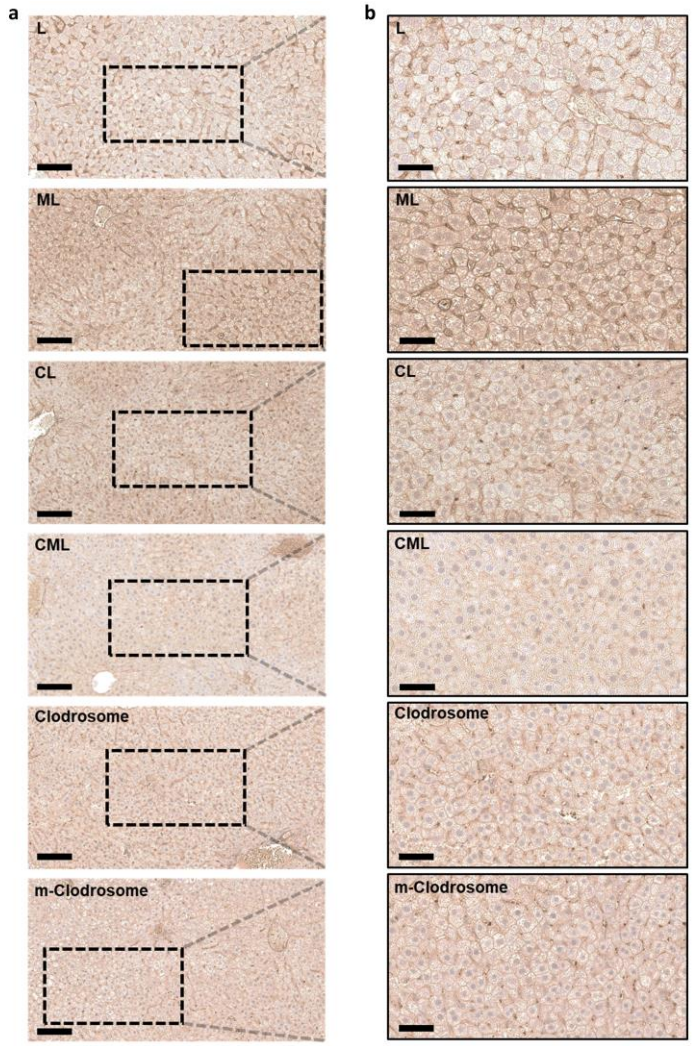

Fig. 12 | M2 macrophage populations in liver tissues using anti-CD206 antibody.

a, Immunohistochemistry stained images of liver tissues from normal mice injected with liposome nanoplatform. Scale bar = 100 μm.

b, Higher magnification images of black-outlined area. Scale bar = 50 μm.

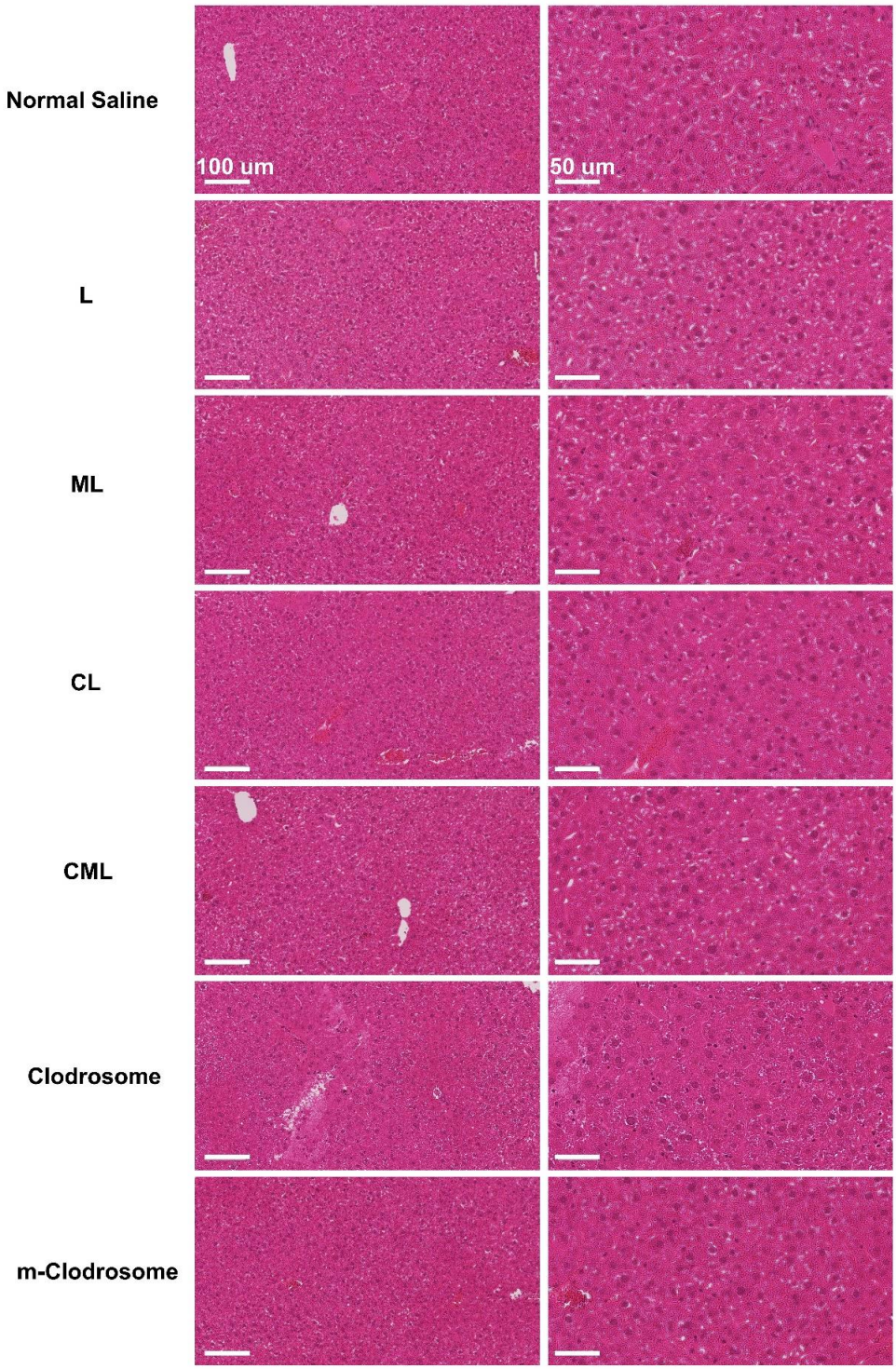

Fig. 13 | Histological analysis of H&E stained sectioned images of the liver tissue treated liposomes.

3.6. Efficacy evaluation of liposome nanoplatform for macrophage depletion in TME ex vivo

To confirm the efficacy of liposome nanoplatform for macrophage depletion in TME compared to positive controls (i.e., Clodrosome® and m-Clodrosome®), we used 4T1 breast cancer cell. This is because it is known that M2 macrophage, a TAM among immune cells, plays an important role in tumor growth, metastasis and angiogenesis in the TME of breast cancer [21]. we conducted histological evaluation of 4T1 tumor tissues using anti-CD206 antibody as M2 macrophage marker. As a result, it was estimated that CML most efficiently blocked tumor progression based on the frequency of M2 macrophages between cancer cells and the degree of staining of the nuclei of cancer cells by hematoxylin (**Fig. 14**). Thus, we could speculate that CML might be efficiently achieved specific targeting of M2 macrophage among TAMs in the TME, and caused macrophage depletion by inducing apoptosis by clodronate that was encapsulated in CML.

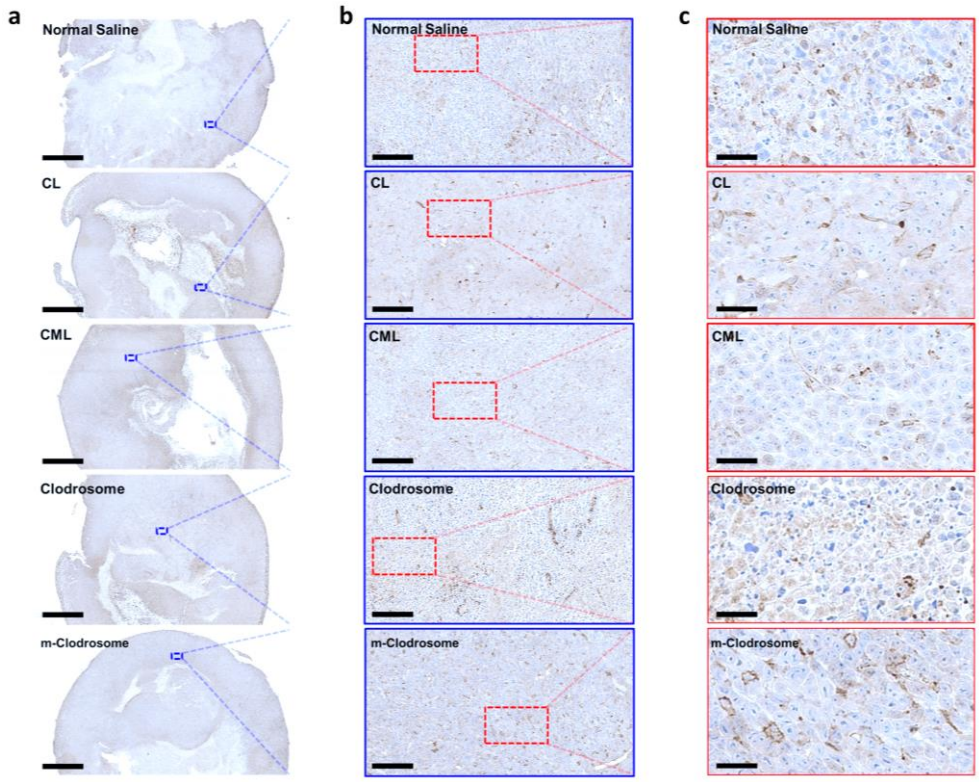

Fig. 14 | M2 macrophage populations in TME using anti-CD206 antibody.

a, Immunohistochemistry stained images of tumor tissues from 4T1-bearing mice injected with liposome nanoplatform. Scale bar = 2000 μm.

b, Higher magnification images of blue-outlined area. Scale bar = 100 μm.

c, Higher magnification images of red-outlined area. Scale bar = 25 μm.

Chapter 4. Conclusion

We developed liposome nanoplatform for effective macrophage depletion in the TME. We found that our liposome nanoplatform presented (1) finely tuned size control (2) high in vivo stability (3) excellent ex vivo M2 macrophage targeting and depleting effect. Furthermore, we found that CML is superior to the already commercialized Clodrosome® and m-Clodrosome® for macrophage depletion. However, there are also some limitations of our liposome nanoplatform. In fact, 100 nm may not be the optimal size for macrophage depletion, since we only confirmed the function of the liposome nanoplatform as a macrophage depleting agent for one size. Therefore, we plan to compare the macrophage depletion effect between liposome nanoplatforms of various sizes through future studies. Meanwhile, it is expected that combination therapy using ICIs and our liposome nanoplatform that can control TME could improve therapeutic efficacy of ICIs by effectively entering ICIs into TME and enhancing their interaction with TAMs. So, we believe that our liposome nanoplatform is an alternative to promising clinical tools for cancer immunotherapy.

Bibliography

1. Sharma P, Allison JP: The future of immune checkpoint therapy. *Science* 2015, 348:56-61.
2. Das S, Johnson DB: Immune-related adverse events and anti-tumor efficacy of immune checkpoint inhibitors. *J Immunother Cancer* 2019, 7:306.
3. Chamseddine AN, Assi T, Mir O, Chouaib S: Modulating tumor-associated macrophages to enhance the efficacy of immune checkpoint inhibitors: A TAM-pting approach. *Pharmacol Ther* 2022, 231:107986.
4. Xiang X, Wang J, Lu D, Xu X: Targeting tumor-associated macrophages to synergize tumor immunotherapy. *Signal Transduct Target Ther* 2021, 6:75.
5. Zeisberger SM, Odermatt B, Marty C, Zehnder-Fjallman AH, Ballmer-Hofer K, Schwendener RA: Clodronate-liposome-mediated depletion of tumour-associated macrophages: a new and highly effective antiangiogenic therapy approach. *Br J Cancer* 2006, 95:272-281.
6. Wu X, Schulte BC, Zhou Y, Haribhai D, Mackinnon AC, Plaza JA, Williams CB, Hwang ST: Depletion of M2-like tumor-associated macrophages delays cutaneous T-cell lymphoma development in vivo. *J Invest Dermatol* 2014, 134:2814-2822.
7. Kraft JC, Freeling JP, Wang Z, Ho RJ: Emerging research and clinical development trends of liposome and lipid nanoparticle drug delivery systems. *J Pharm Sci* 2014, 103:29-52.
8. Beltrán-Gracia E, López-Camacho A, Higuera-Ciapara I, Velázquez-Fernández JB, Vallejo-Cardona AA: Nanomedicine review: clinical developments in liposomal applications. *Cancer Nanotechnology* 2019, 10.
9. Danaei M, Dehghankhold M, Ataei S, Hasanzadeh Davarani F, Javanmard R, Dokhani A, Khorasani S, Mozafari MR: Impact of Particle Size and Polydispersity Index on the Clinical Applications of Lipidic Nanocarrier Systems. *Pharmaceutics* 2018, 10.
10. Lee W, Jeon M, Choi J, Oh C, Kim G, Jung S, Kim C, Ye SJ, Im HJ: Europium-Diethylenetriaminepentaacetic Acid Loaded Radioluminescence Liposome Nanoplatform for Effective Radioisotope-Mediated Photodynamic Therapy. *ACS Nano* 2020, 14:13004-13015.
11. Jeon M, Kim G, Lee W, Baek S, Jung HN, Im HJ: Development of theranostic dual-layered Au-liposome for effective tumor targeting and photothermal therapy. *J Nanobiotechnology* 2021, 19:262.
12. Park CR, Kim HY, Song MG, Lee YS, Youn H, Chung JK, Cheon GJ, Kang KW: Efficacy and Safety of Human Serum Albumin-Cisplatin Complex in U87MG Xenograft Mouse Models. *Int J Mol Sci* 2020, 21.

13. Jeong S, Park JY, Cha MG, Chang H, Kim YI, Kim HM, Jun BH, Lee DS, Lee YS, Jeong JM, et al: Highly robust and optimized conjugation of antibodies to nanoparticles using quantitatively validated protocols. *Nanoscale* 2017, 9:2548-2555.
14. Hwang DW, Choi H, Jang SC, Yoo MY, Park JY, Choi NE, Oh HJ, Ha S, Lee YS, Jeong JM, et al: Noninvasive imaging of radiolabeled exosome-mimetic nanovesicle using (99m)Tc-HMPAO. *Sci Rep* 2015, 5:15636.
15. Gupta A, Shin JH, Lee MS, Park JY, Kim K, Kim JH, Suh M, Park CR, Kim YJ, Song MG, et al: Voxel-Based Dosimetry of Iron Oxide Nanoparticle-Conjugated (177)Lu-Labeled Folic Acid Using SPECT/CT Imaging of Mice. *Mol Pharm* 2019, 16:1498-1506.
16. Sercombe L, Veerati T, Moheimani F, Wu SY, Sood AK, Hua S: Advances and Challenges of Liposome Assisted Drug Delivery. *Front Pharmacol* 2015, 6:286.
17. Olusanya TOB, Haj Ahmad RR, Ibegbu DM, Smith JR, Elkordy AA: Liposomal Drug Delivery Systems and Anticancer Drugs. *Molecules* 2018, 23.
18. Danenberg HD, Fishbein I, Gao J, Monkkonen J, Reich R, Gati I, Moerman E, Golomb G: Macrophage depletion by clodronate-containing liposomes reduces neointimal formation after balloon injury in rats and rabbits. *Circulation* 2002, 106:599-605.
19. van Rooijen N, Sanders A, van den Berg TK: Apoptosis of macrophages induced by liposome-mediated intracellular delivery of clodronate and propamidine. *J Immunol Methods* 1996, 193:93-99.
20. Van Rooijen N, Sanders A: Liposome mediated depletion of macrophages: mechanism of action, preparation of liposomes and applications. *J Immunol Methods* 1994, 174:83-93.
21. Radharani NNV, Yadav AS, Nimma R, Kumar TVS, Bulbule A, Chanukuppa V, Kumar D, Patnaik S, Rapole S, Kundu GC: Tumor-associated macrophage derived IL-6 enriches cancer stem cell population and promotes breast tumor progression via Stat-3 pathway. *Cancer Cell Int* 2022, 22:122.
22. Shao J, Ma JKH: Characterization of a mannosylphospholipid liposome system for drug targeting to alveolar macrophages. *Drug Deliv* 2008, 4:43-48.
23. Ye J, Yang Y, Dong W, Gao Y, Meng Y, Wang H, Li L, Jin J, Ji M, Xia X, et al: Drug-free mannosylated liposomes inhibit tumor growth by promoting the polarization of tumor-associated macrophages. *Int J Nanomedicine* 2019, 14:3203-3220.
24. Jeong HS, Na KS, Hwang H, Oh PS, Kim DH, Lim ST, Sohn MH, Jeong HJ: Effect of space length of mannose ligand on uptake of mannosylated liposome in RAW 264.7 cells: In vitro and in vivo studies. *J Biomed Mater Res A* 2014, 102:4545-4553.
25. Lodhi NA, Park JY, Kim K, Kim YJ, Shin JH, Lee YS, Im HJ, Jeong JM, Khalid M, Cheon GJ, et al: Development of (99m)Tc-Labeled Human Serum Albumin with Prolonged Circulation by Chelate-then-Click Approach: A Potential Blood Pool Imaging Agent. *Mol Pharm* 2019,

16:1586-1595.
26. Takayama Y, Kusamori K, Nishikawa M: Click Chemistry as a Tool for Cell Engineering and Drug Delivery. *Molecules* 2019, 24.
27. Oude Blenke E, Klaasse G, Merten H, Pluckthun A, Mastrobattista E, Martin NI: Liposome functionalization with copper-free "click chemistry". *J Control Release* 2015, 202:14-20.
28. Park JY, Song MG, Kim WH, Kim KW, Lodhi NA, Choi JY, Kim YJ, Kim JY, Chung H, Oh C, et al: Versatile and Finely Tuned Albumin Nanoplatform based on Click Chemistry. *Theranostics* 2019, 9:3398-3409.
29. Chung H, Park JY, Kim K, Yoo RJ, Suh M, Gu GJ, Kim JS, Choi TH, Byun JW, Ju YW, et al: Circulation Time-Optimized Albumin Nanoplatform for Quantitative Visualization of Lung Metastasis via Targeting of Macrophages. *ACS Nano* 2022, 16:12262-12275.
30. Gonzalez Gomez A, Syed S, Marshall K, Hosseinidoust Z: Liposomal Nanovesicles for Efficient Encapsulation of Staphylococcal Antibiotics. *ACS Omega* 2019, 4:10866-10876.
31. Bozzuto G, Molinari A: Liposomes as nanomedical devices. *Int J Nanomedicine* 2015, 10:975-999.
32. Seo HJ, Nam SH, Im HJ, Park JY, Lee JY, Yoo B, Lee YS, Jeong JM, Hyeon T, Kim JW, et al: Rapid Hepatobiliary Excretion of Micelle-Encapsulated/Radiolabeled Upconverting Nanoparticles as an Integrated Form. *Sci Rep* 2015, 5:15685.
33. Garnett MC, Kallinteri P: Nanomedicines and nanotoxicology: some physiological principles. *Occup Med (Lond)* 2006, 56:307-311.
34. Ait-Mohand S, Fournier P, Dumulon-Perreault V, Kiefer GE, Jurek P, Ferreira CL, Benard F, Guerin B: Evaluation of 64Cu-labeled bifunctional chelate-bombesin conjugates. *Bioconjug Chem* 2011, 22:1729-1735.
35. Kim S, Jeong JM, Hong MK, Jang JJ, Lee J, Lee DS, Chung JK, Lee MC: Differential receptor targeting of liver cells using 99mTc-neoglycosylated human serum albumins. *Arch Pharm Res* 2008, 31:60-66.
36. Colino CI, Lanao JM, Gutierrez-Millan C: Targeting of Hepatic Macrophages by Therapeutic Nanoparticles. *Front Immunol* 2020, 11:218.
37. Nguyen-Lefebvre TAH, A.: Kupffer Cell Metabolism and Function. 2015.
38. Dixon LJ, Barnes M, Tang H, Pritchard MT, Nagy LE: Kupffer cells in the liver. *Compr Physiol* 2013, 3:785-797.
39. Lombardo D, Calandra P, Barreca D, Magazu S, Kiselev MA: Soft Interaction in Liposome Nanocarriers for Therapeutic Drug Delivery. *Nanomaterials (Basel)* 2016, 6.
40. Zamboni WC: Concept and clinical evaluation of carrier-mediated anticancer agents. *Oncologist* 2008, 13:248-260.
41. Duan Z, Luo Y: Targeting macrophages in cancer immunotherapy. *Signal Transduct Target Ther* 2021, 6:127.
42. Gustafson HH, Holt-Casper D, Grainger DW, Ghandehari H:

Nanoparticle Uptake: The Phagocyte Problem. *Nano Today* 2015, 10:487-510.

Abstract in Korean

서론: 면역관문억제제를 이용한 면역치료법은 암세포를 직접 죽이는 것이 아니라 종양미세환경 내에 있는 면역세포를 활성화시켜 항암면역을 유도하는 치료법이다. 하지만, 면역관문억제제의 임상적 성공은 환자의 약 1/3만이 지속적인 반응을 보였으며, 그마저도 결국 재발하는 것으로 보고되었다. 이에 면역관문억제제의 치료 효과를 높이기 위한 다양한 병용요법이 연구되고 있다. 그 중 대두되고 있는 병용요법으로는 종양 미세 환경에서 종양 관련 대식세포를 조절한 후에 면역관문억제제로 치료하는 것이 있다. 종양 미세 환경의 종양 관련 대식세포 중 M2 대식세포는 종양 성장을 촉진한다고 알려져 있다. 이러한 종양 관련 대식세포를 고갈시키기 위해 상업적으로 사용되는 제제는 Clodrosome® 및 m-Clodrosome®이 있다. 그러나 이 제제의 불균일성으로 인해 임상적 사용이 제한된다. 따라서, 본 연구에서는 M2 대식세포인 종양 관련 대식세포를 표적 및 고갈시킬 수 있는 리포좀 대식세포 고갈제를 개발하여 임상적으로 면역관문억제제와의 병용요법으로 활용하고자 하였다. 본 연구의 목적은 Clodrosome® 및 m-Clodrosome® 대비 이 연구를 통해 개발한 리포좀 대식세포 고갈제의 우수성을 입증하는 것이다.

방법: 클릭 화학 기반 리포좀 나노플랫폼은 두 단계로 합성되었다. 첫째, 박막 수화 및 압출에 의해 리포좀을 합성하였다. 둘째, 클릭 화학 반응을 사용하여 아자이드 기능화 킬레이트제, 만노스, 형광 염료를 리포좀의 DBCO와 결합시켰다. 기능화된 리포좀의 생체분포 및 대식세포 제거 능력은 쥐에서 입증하였다.

결과: 우리는 효과적인 대식세포 제거를 위해 크기가 일정하고

클로드로네이트로 캡슐화된 4가지 유형의 클릭 화학 기반 리포좀 나노플랫폼을 개발한 후, Man-N_3 및 금속 동위원소 ^{64}Cu 표지를 진행했다. Man-N_3를 사용한 기능화는 M2 대식세포의 표적화 능력을 향상시키고 ^{64}Cu 표지는 리포좀의 생체 내 양전자 방출 단층 촬영 (PET) 이미징을 가능하게 했다. 기능화된 리포좀 나노플랫폼은 생리학적 조건에서 안정적이었고 PET를 이용하여 생체분포의 차이를 확인하였다. 또한, 리포좀 나노플랫폼 중 클로드로네이트 캡슐화 만노실화 리포좀 (CML)은 Clodrosome® 및 m-Clodrosome®과 비교하여 생체 외 정상 간 및 종양 미세환경 (TME)에서 M2 대식세포를 효과적으로 고갈시켰다.

결론: 미세하게 조정된 크기 조절, 높은 생체 내 안정성 및 우수한 생체 외 M2 대식세포 표적화 및 제거 효과를 기반으로 개발된 리포좀 나노플랫폼은 유망한 대식세포 제거제가 될 수 있을 것으로 사료된다.

주요어 : 리포좀, 대식세포, 클로드로네이트, 분자 이미징, 클릭 화학

학번 : 2021-24307